Atmos. Chem. Phys. Discuss., 14, 6501–6536, 2014
www.atmos-chem-phys-discuss.net/14/6501/2014/
doi:10.5194/acpd-14-6501-2014
© Author(s) 2014. CC Attribution 3.0 License.

Atmospheric Chemistry and Physics Discussions

This discussion paper is/has been under review for the journal Atmospheric Chemistry and Physics (ACP). Please refer to the corresponding final paper in ACP if available.

Evaluation of tropospheric SO_2 retrieved from MAX-DOAS measurements in Xianghe, China

T. Wang[1,2], F. Hendrick[2], P. Wang[1], G. Tang[1], K. Clémer[2,*], H. Yu[2], C. Fayt[2], C. Hermans[2], C. Gielen[2], G. Pinardi[2], N. Theys[2], H. Brenot[2], and M. Van Roozendael[2]

[1]Institute of Atmospheric Physics, Chinese Academy of Sciences, Beijing, China
[2]Belgian Institute for Space Aeronomy, Brussels, Belgium
[*]now at: Instituut voor Sterrenkunde, Katholieke Universiteit Leuven, Leuven, Belgium

Received: 7 January 2014 – Accepted: 26 February 2014 – Published: 11 March 2014

Correspondence to: F. Hendrick (franch@oma.be)

Published by Copernicus Publications on behalf of the European Geosciences Union.

Abstract

Ground-based Multi-Axis Differential Optical Absorption Spectroscopy (MAX-DOAS) measurements of sulfur dioxide (SO_2) have been performed at the Xianghe station (39.75° N, 116.96° E) located at ~ 50 km southeast of Beijing from March 2010 to February 2013. Tropospheric SO_2 vertical profiles and corresponding vertical column densities (VCDs), retrieved by applying the Optimal Estimation Method to the MAX-DOAS observations, have been used to study the seasonal and diurnal cycles of SO_2, in combination to correlative measurements from in situ instruments, as well as meteorological data. A marked seasonality was observed in both SO_2 VCD and surface concentration, with a maximum in winter (February) and a minimum in summer (July). This can be explained by the larger emissions in winter due to the domestic heating and more favorable meteorological conditions for the accumulation of SO_2 close to the ground during this period. Wind speed and direction are also found to be two key factors in controlling the level of the SO_2-related pollution at Xianghe. In the case of east or southwest wind, the SO_2 concentration rises with the increase of the wind speed, since heavy polluting industries are located to the east and southwest of the station. In contrast, when wind comes from other directions, the stronger the wind, the less SO_2 is observed. Regarding the diurnal cycle, the SO_2 amount is larger in the early morning and late evening and lower at noon, in line with the diurnal variation of pollutant emissions and atmospheric stability. The observed diurnal cycles of MAX-DOAS SO_2 surface concentration are also in very good agreement (correlation coefficient close to 0.9) with those from collocated in-situ data, demonstrating the reliability and robustness of our retrieval.

1 Introduction

Sulfur dioxide (SO_2), one of the most common air pollutants, is of major concern in pollution control acts (Gauderman et al., 2000). In China, the Ministry of Environmental

Protection (MEP) lists SO_2 as one of the three conventional pollutants, together with NO_2 and PM_{10}, and daily averaged SO_2 concentrations were used as an indicator to quantify the level of pollution (Yan et al., 2010). This trace gas is predominantly produced by the burning of fossil fuels including oil and coal, and the smelting of mineral ores that contain sulfur (Yan et al., 2005; Zhao et al., 2012). Furthermore, SO_2 contributes in a large extent to the process of acidification resulting in acid rain and to the formation of sulfate aerosols, both of which cause human health damages, building surface corrosion, and visibility reduction. In particular, the secondary pollutant sulfate aerosols generated by SO_2 are the primary source of fine solid particles in cities, which are also responsible for severe air pollution issues (Meng et al., 2009). In addition, the on-going industrial development, population growth, and heavy traffic contribute to higher energy consumption and therefore, to an increase in SO_2 emissions into the atmosphere (Wu et al., 2013). Consequently, in order to meet urgent demand in China to improve and control air quality, as well as to promote sustainable development, it is of the greatest importance to study the evolution of a pollutant like SO_2 and to identify its possible origins.

So far, the SO_2 surface concentration has been monitored using in-situ and long-path DOAS (Differential Optical Absorption Spectroscopy) instruments (Meng et al., 2009), while satellite sensors like GOME, SCIAMACHY, GOME-2, OMI, OMPS, and IASI have shown their ability to measure the SO_2 vertical column density (VCD) over polluted areas (see e.g. Eisinger and Burrows, 1998; Krotkov et al., 2006; Lee et al., 2009; Nowlan et al., 2011; Fioletov et al., 2013; Yang et al., 2013; Boynard et al., 2014). During the last decade, a new remote sensing technique called MAX-DOAS (Multi-Axis Differential Optical Absorption Spectroscopy) has been developed, providing information on both VCD and vertical distribution of trace gases in the troposphere (Hönninger et al., 2004; Platt and Stutz, 2008). It is based on the measurement of sunlight scattered at multiple elevation angles towards the horizon, thus increasing the sensitivity to absorbers present close to the ground compared to the zenith viewing geometry (Hönninger et al., 2004). MAX-DOAS studies published so far have been mainly focused

on the retrieval of NO_2 (e.g. Wittrock et al., 2004; Vlemmix et al., 2010; Frins et al., 2012; Hendrick et al., 2014; Ma et al., 2013; Wang et al., 2014), halogen oxides like BrO and IO (e.g. Frieß et al., 2011; Großmann et al., 2013), formaldehyde (e.g. Heckel et al., 2005; Wagner et al., 2011), and aerosols (e.g. Wagner et al., 2004; Frieß et al., 2006; Clémer et al., 2010). Regarding SO_2, only little efforts have been dedicated to the retrieval and monitoring of this species from MAX-DOAS measurements (Irie et al., 2011; Wu et al., 2013), despite the fact that as for other trace gases like NO_2, HCHO, and BrO, the combination of both surface concentration and VCD retrievals makes MAX-DOAS a useful technique for validating SO_2 satellite data.

Here we present three years (March 2010–February 2013) of continuous MAX-DOAS SO_2 observations at the Xianghe Observatory, China (39.75° N, 116.96° E), located at about 50 km South-East of Beijing, at the borders among Beijing, Tangshan and Tianjin (see Fig. 1). The station is operated by the Institute of Atmospheric Physics (IAP)/Chinese Academy of Sciences (CAS) while the MAX-DOAS instrument was developed by the Belgian Institute for Space Aeronomy (BIRA-IASB) and validated in several intercomparison exercises, in particular as part of the international Cabauw Intercomparison of Nitrogen Dioxide measuring Instruments (CINDI, Roscoe et al., 2010) and more recently a national Chinese MAX-DOAS instruments intercomparison campaign held in Xianghe (Wang et al., 2013). SO_2 MAX-DOAS observations are used here in combination with in-situ measurements as well as conventional meteorological data (temperature, humidity, wind direction and speed) to investigate the seasonal and diurnal cycles of SO_2 vertical profiles and VCDs. The paper is divided into three main Sections. In Sect. 2, the SO_2 measurements are described, including the DOAS analysis, vertical profile retrieval, and retrieval verification through comparison with in situ data. The seasonal and diurnal cycles of SO_2 are investigated in Sect. 3. Finally, conclusions are given Sect. 4.

2 Data

2.1 Instrument

The MAX-DOAS instrument operated at the Xianghe Observatory consists of three components: a thermo-regulated box containing two spectrometers, an optical head mounted on a sun tracker, and two computers for instrument control and data storage (Clémer et al., 2010). The optical head and the two spectrometers are linked by two-way splitter optical fibers (Clémer et al., 2010; Wang et al., 2013). This setup is capable of measuring scattered as well as direct sunlight. One spectrometer works in the UV region (300 to 390 nm) and its instrumental function is close to a Gaussian with a full width at half maximum (FWHM) of 0.4 nm. The other spectrometer covers the visible wavelength range from 400 to 720 nm with a FWHM equal to 0.9 nm. During the observation, the azimuth direction of the telescope is fixed to the North. A full MAX-DOAS scan consists of 9 elevation viewing angles (2°, 4°, 6°, 8°, 10°, 12°, 15°, 30°, and 90°) and lasts about 15 min (Clémer et al., 2010). The 3 year data set investigated in this study covers the March 2010 to February 2013 period.

2.2 DOAS analysis

Scattered-sunlight spectra measured at different elevation angles (EVAs) are analyzed using the DOAS technique (Platt and Stutz, 2008) where high-frequency molecular absorption structures in the UV and visible regions of the spectrum are exploited to detect and quantify a number of key atmospheric gases such as SO_2.

In this work, the spectra obtained from MAX-DOAS observations are analyzed using the QDOAS spectral-fitting software suite developed at BIRA-IASB (http://uv-vis.aeronomie.be/software/QDOAS/). QDOAS calculates the SO_2 differential slant column densities (DSCDs), which are defined as the difference between the trace-gas concentration integrated along the effective light path and the amount of the absorber in a measured reference spectrum. This self-calibration ensures very good stability of the

measurements, in contrast to in situ instruments which require calibration on a regular basis. In practice, for tropospheric studies, the zenith spectrum of each scan is frequently chosen as reference, in this way removing the contribution of the stratosphere in off-axis DSCDs.

According to the sensitivity tests we performed, the most suitable fitting window for SO_2 is found to be 305–317.5 nm. This choice is based on the fact that SO_2 displays strong absorption differential structures in this interval while ozone interferences can still be managed until moderately high solar zenith angles (approximately 75°). The DOAS analysis settings, including the trace-gas cross-sections, are described in Table 1. The other trace gases taken into account in the fitting process are NO_2, O_3, as well as the Ring effect (Grainger and Ring, 1962; Chance and Spurr, 1997). A fifth-order polynomial is used to fit the low-frequency spectral structure due to Rayleigh and Mie scattering and instrumental effects. Figure 2 shows a typical example of a DOAS fit for SO_2 at 43° SZA (solar zenith angle). We see that the residual is small, ranging from -2×10^{-3} to 2×10^{-3}, which indicates a limited retrieval error. In this illustrative case, the retrieved SO_2 DSCD is 7.27×10^{16} molec cm^{-2}.

2.3 Profile retrieval

SO_2 vertical profiles are retrieved for each MAX-DOAS scan by applying the bePRO profiling tool developed at BIRA-IASB (Clémer et al., 2010; see also Hendrick et al., 2014) to the corresponding DSCDs measured at the different EVAs. bePRO is based on the Optimal Estimation Method (Rodgers, 2000) and includes the LIDORT radiative transfer model (RTM) as a forward model. A two-step approach is implemented in bePRO: first, aerosol extinction profiles are retrieved from measured O_4 DSCDs. This step is needed because the aerosols strongly influence the effective light path in the atmosphere and therefore the absorption by trace gases like SO_2. Secondly, bePRO is applied to measured trace-gas DSCDs using the retrieved aerosol extinction profiles for the radiative transfer calculations (see below).

Aerosol extinction and SO_2 vertical profiles $\boldsymbol{x}$ are obtained by means of an iterative approach using the following equation:

$$\boldsymbol{x}_{i+1} = \boldsymbol{x}_i + \left(\mathbf{S}_a^{-1} + \mathbf{K}_i^T \mathbf{S}_\varepsilon^{-1} \mathbf{K}_i\right)^{-1} \cdot \left[\mathbf{K}_i^T \mathbf{S}_\varepsilon^{-1} (\boldsymbol{y} - \mathbf{F}(x_i)) - \mathbf{S}_a^{-1} (\boldsymbol{x}_i - \boldsymbol{x}_a)\right] \quad (1)$$

where $\boldsymbol{y}$ is the observation vector with the DSCDs at the different EVAs, $\mathbf{F}$ is the forward model describing the physics of the measurements, $\mathbf{K}$ is the weighting function, expressing the sensitivity of the measurements to changes in the aerosol extinction or SO_2 vertical profile and calculated on-line by the LIDORT RTM, $\mathbf{S}_\varepsilon$ is the measurement uncertainty covariance matrix, $\boldsymbol{x}_a$ and $\mathbf{S}_a$ are the a priori vertical profile and its corresponding error covariance matrix. A priori information is needed in the OEM method in order to reject unrealistic solutions compatible with the measurements. Another important quantity in the OEM is the averaging kernel matrix $\mathbf{A}$, which represents the sensitivity of the retrieval to the true state. More specifically, each element $\mathbf{A}_{ij}$ in the matrix $\mathbf{A}$ describes the sensitivity of the retrieval at ith level to the true states at the different altitude levels j. Furthermore, the trace of the matrix $\mathbf{A}$ gives the degrees of freedom of signal (DFS), which corresponds to the number of independent pieces of information contained in the measurements. Due to the nonlinearity of the inverse problem in case of aerosols, the solution to Eq. (1) must be iterated until satisfactory convergence is achieved between measured DSCDs and those calculated using the retrieved aerosol extinction vertical profile.

Regarding the choice of the a priori profile $\boldsymbol{x}_a$, a fixed aerosol extinction profile taken from the LOWTRAN climatology is selected for the aerosol profile retrieval step (Clémer et al., 2010). In case of SO_2, exponentially decreasing a priori profiles with a fixed scaling height of 0.5 km have been constructed according to the following expression:

$$\boldsymbol{x}_a(z) = \frac{\mathrm{VCD}_a}{\mathrm{SH}} \mathrm{e}^{-\frac{z}{\mathrm{SH}}} \quad (2)$$

where $\boldsymbol{x}_a(z)$ is the a priori profile, SH the scaling height (0.5 km), and VCD_a is the a priori vertical column density derived using the geometrical approximation method,

i.e. the SO_2 layer is assumed to be located below the scattering altitude at 30° EVA, so that tropospheric SO_2 VCDs can be derived by applying a geometrical air mass factor (AMF) to measured 30° EVA DSCDs (Hönninger et al., 2004; Brinksma et al., 2008; see also Hendrick et al., 2014). Since the DOAS fitting intervals are different for SO_2 and aerosols, the aerosol extinction profiles utilized as input for the calculation of SO_2 weighting functions have been derived by converting the AODs retrieved in the 338–370 nm wavelength range to the 305–317.5 nm interval using the Ångström formula (Cachorro et al., 2000), and assuming an exponentially decreasing profile shape with a SH of 0.5 km (see Eq. 2). The single scattering albedo and phase function of aerosols at 360 nm required by bePRO for retrieving aerosol extinction profiles are calculated off-line based on the aerosol size distribution and refractive index retrieved from collocated CIMEL sunphotometer measurements (Holben et al., 1998). The temperature-pressure profiles are obtained from the US standard atmosphere. Finally, $\mathbf{S}_\varepsilon$ and $\mathbf{S}_a$ matrices as well as the retrieval altitude grid are similar as in Clémer et al. (2010) and Hendrick et al. (2014), i.e. in the case of the altitude grid: ten layers of 200 m thickness between 0 and 2 km, two layers of 500 m between 2 and 3 km and 1 layer between 3 and 4 km.

Figure 3 shows an example of a SO_2 profile retrieval (Xianghe, 29 September 2010, 10:15 LT). Figure 3a compares the a priori and retrieved profiles; Fig. 3b shows an example of fit results, i.e. the comparison between measured DSCDs and those calculated from the retrieved profile. The quality of the profile retrieval is checked for each scan by calculating the Root Mean Square Error (RMS) between observed and calculated DSCDs. All retrievals based on the following selection criteria have been selected: RMS < 15 %, DFS > 0.7, and negative values not allowed. For each year, the number of selected retrievals using these criteria reaches ~75 % of the total number of scans.

Also shown in Fig. 3 are the smoothing and noise errors (c) and the averaging kernels (d). Regarding the errors, the smoothing error limits the ability of the retrieval to obtain solutions far from the a priori, while the noise error is related to the propagation of the noise in the measurements into the retrieval (Rodgers, 2000). From Fig. 3c, we see that the smoothing error is significantly larger than the noise error, except in the 0–200 m

layer. The averaging kernels show that the retrieval is mainly sensitive to the layer close to the surface in addition to the total vertical column. In this example, the DFS is about 2.1, suggesting that two independent pieces of information can be determined from the measurements.

The error budget is presented in Table 2. Uncertainty related to aerosols is estimated by retrieving SO_2 profiles using retrieved AOD plus their corresponding error (i.e. the sum of smoothing and noise errors plus a 20 % error due to the uncertainty on the O_4 cross sections; see Clémer et al., 2010) as input and comparing the results to the standard retrievals. The uncertainty on the SO_2 cross sections is set to 5 %, as suggested by Vandaele et al. (1994). The uncertainty on the a priori profiles is estimated by taking SH = 1 km in Eq. (2) instead of 0.5 km in the standard retrieval. The total uncertainty is calculated by adding the different terms in Gaussian quadrature.

Monthly-mean SO_2 profiles are shown in Fig. 4. There is a maximum SO_2 concentration at the surface for each profile, except in November–December where the maximum is located in the 200–400 m layer. The largest vertical gradient is observed in February and November, the smallest in July and August, which is due to the difference in SO_2 concentration near ground for the different months. This will be discussed in detail below.

Figure 5 shows the seasonal mean of diurnal cycle of DFS. The diurnal distribution in any season shows a single peak at mid-day due to the fact that the retrieval error at late evening or early morning overweights that at noon. If we compare the DFS around noon among the different seasons, values in summer are lower compared to the other seasons due to the lower SO_2 amounts observed during this period.

2.4 SO_2 surface concentration retrieval verification

For verification purpose, our retrieved SO_2 surface concentrations have been compared to measurements from a modified commercial in-situ instrument, based on pulsed UV fluorescence technology (Thermo Environmental Instruments Model 43C) (Li et al., 2007). Comparison results for December 2011 when the in-situ instrument

was freshly calibrated are shown in Fig. 6. Hourly and daily averages of SO_2 concentration are plotted in Fig. 6a and b, respectively. A good agreement is obtained with a correlation coefficient of 0.8 and a slope of 0.9.

In Fig. 7, the daytime variations of the MAX-DOAS and in-situ SO_2 surface concentration are compared for 9 continuous days. A very good agreement is found between both data sets, indicating the good overall reliability and the robustness of our MAX-DOAS retrievals.

3 Results and discussion

Based on the SO_2 profiles retrieved for the period from March 2010 to February 2013, we have investigated the daily and seasonal variations of the SO_2 VCD and surface concentration and the possible influence of meteorological conditions, including atmospheric stability, wind direction and speed. We have adopted the following convention for the season: spring is from March to May, summer from June to August, autumn from September to November, and winter from December to February.

3.1 Seasonal variation of SO_2

Figure 8a shows that the SO_2 VCD is highly correlated with concentration close to the ground (correlation coefficient of 0.88). From Fig. 8b, we see that the temporal evolutions of SO_2 VCD and concentration are very similar, consistent with the fact that the SO_2 emission sources are located near the ground.

The monthly averaged SO_2 VCD and surface concentrations are shown in Fig. 9. Both show a marked seasonal signature with a maximum in winter and a minimum in summer, implying that SO_2 originates mainly from human sources rather than natural ones (Lin et al., 2011). Generally, the fluctuations of any atmospheric pollutant in a region of interest can be mainly attributed to three factors: emission level, residence time, and atmospheric transport (Wang et al., 2010; Lin et al., 2011). From the perspective

of emission level, firstly, owing to enhanced domestic heating and associated coal and oil consumption in winter, the heating-related emissions of SO_2 are much larger during this period than in summer. Secondly, the residence time, defined as the rate of removal mechanisms, also plays an important role in determining the seasonal variation of SO_2 concentrations (Lee et al., 2011). Processes responsible for the removal of SO_2 involve dry and wet deposition and homogeneous or inhomogeneous gas-phase reactions leading to the production of H_2SO_4 or sulfate (Tu et al., 2004). As shown in Fig. 10, the relative humidity is lower in winter, so that the removal of SO_2 through wet deposition is not as substantial as in summer. Thirdly, the transport can also influence the evolution of SO_2 at a given location. Although in winter the wind is stronger at Xianghe, the emissions also increase during the same period. In addition, the reduced atmospheric boundary layer height and frequent temperature inversion events result in an accumulation of SO_2 in the lower troposphere (Meng et al., 2009). In summary, the aforementioned three factors jointly lead to the observed seasonal pattern of SO_2 concentration in Xianghe.

From Fig. 9, we see that the amount of SO_2 strongly increases in November with respect to October, as a consequence of increasing domestic heating (November is the beginning of the domestic heating season). Moreover, the higher wind speed observed in December (see Fig. 10) leads to a decrease of SO_2 during this month due to more efficient diffusion and dilution effects. Finally, it is also noticeable that SO_2 in January 2011 is remarkably lower than that in other years. This will be further discussed below.

3.2 Impact of meteorological conditions

Because of the high correlation coefficient and similar seasonal variations of the SO_2 VCD and concentration, we decided to investigate the impact of meteorological conditions on VCDs only. The variation of the SO_2 VCD is closely linked not only to the spatial distribution of emission sources but also to meteorological conditions including wind (speed and direction) and precipitation. As shown in Fig. 10, in general, the

variations of temperature and humidity appear to exhibit similar behavior from year to year. This suggests that the contribution of the wind speed and direction as driver for the SO_2 VCD variation is probably different over the different years investigated here. For this purpose, we further explore the relationship between SO_2 and wind (speed and direction), as displayed in Fig. 11. It can be seen that the amount of SO_2 is strongly dependent on the wind direction: high VCDs are prominent when the winds blow from the east, because Tangshan, a heavy industrial city releasing large amounts of SO_2, is situated to the east of Xianghe; in contrast, the north-west direction corresponds to a minimum in SO_2 VCD, since it is a mountain area, characterized by much less emissions than in Xianghe. The wind therefore contributes significantly to the dispersion of the pollutants, as expected.

We further assess the dependence of SO_2 on wind speed for a given wind direction. As can be seen in Fig. 11b, the VCD can vary considerably, even for the same wind direction. One can conclude that the SO_2 column is inversely proportional to the wind speed in the case of east and south-west winds, since high-emission industrial areas and Tangshan are located to the south-west and east of Xianghe, respectively. In addition, the SO_2 content in Xianghe is more sensitive to the emission sources in Tangshan (E) than in Beijing (WNW), which is consistent with the fact that Beijing has taken regulatory actions to reduce air pollution through traffic-control measures and the closure of heavy polluting industries initiated before the 2008 Olympic Games (Yu et al., 2010).

The annual cycles of SO_2 are generally in good agreement among the different years. However, the SO_2 VCD in January 2011 drastically deviates by up to 30 % from the values during the same month in 2012 and 2013, which is also the case in May 2012. Wind roses in Fig. 12 reveal that the inter-annual variability of wind speed and direction is responsible for the significantly different SO_2 VCD in January 2011. During that month, the frequency of north-west winds reaches 70 % and wind speed predominantly exceed $5\,m\,s^{-1}$. As mentioned above, the strong northwesterly wind favors the atmospheric dispersion of pollutants. Consequently, the SO_2 VCDs are generally lower than $4 \times 10^{16}\,molec\,cm^{-2}$. For January 2012 and 2013, uniformly distributed wind on each

side and low velocity ($< 5\,m\,s^{-1}$, frequency $> 50\,\%$) jointly result in relatively high SO_2 VCDs compared to January 2011. Similar features can explain the May 2012 case.

3.3 Diurnal cycle

In Fig. 13, we further compare the diurnal cycles of SO_2 VCDs for the different seasons. Since the sunshine duration is different in the four seasons, the available time period for MAX-DOAS observations also differs: 07:30–17:30 LT in spring and autumn, 06:30–18:30 LT in summer, and 08:30–16:30 LT in winter. As can be seen, the diurnal cycles for all years are very consistent, especially in summer. In spring and autumn, the retrieved SO_2 VCDs in autumn 2011 and spring 2012 are significantly higher than those during the same period of the other years due to the anomalous VCD values in November 2011 and May 2012. Furthermore, the amplitude of the SO_2 VCD diurnal cycle, which shows a minimum at noon and a maximum in the morning and late afternoon, is larger in winter. This can be explained by more frequent temperature-inversion events and a strengthened diurnal variation of emission sources during this period (Meng et al., 2009).

It should be noted that similar investigations have been done for NO_2 (Wang et al., 2014). One can conclude that both NO_2 and SO_2 display a similar seasonal variation and are impacted in the same way by meteorological conditions. However, SO_2 abundances are always higher than NO_2 ones and their diurnal cycles are different, especially in winter and summer: SO_2 has a more pronounced diurnal cycle than NO_2 in winter which is in line with the known diurnal cycle of burning of fossil fuels for heating and atmospheric stability, and the photochemical reaction activity leads to an obvious decrease of NO_2 during daytime in summer. (Wang et al., 2008; Meng et al., 2009; Lin et al., 2011).

4 Summary and conclusions

Tropospheric SO_2 vertical profiles and corresponding column densities at the Xianghe station have been retrieved by applying an OEM-based profiling tool to continuous ground-based MAX-DOAS observations from March 2010 to February 2013. The 305–317.5 nm wavelength range was found to be the most suitable fitting window for near-noon DOAS analysis of SO_2. For verification purpose, retrieved SO_2 surface concentrations have been compared to collocated in-situ data. An excellent agreement was found, with correlation coefficient and slope close to 0.9, demonstrating the reliability and robustness of our retrievals.

These MAX-DOAS measurements have been used to investigate the seasonal and diurnal cycles of SO_2 vertical columns and surface concentrations, in combination with conventional meteorological data (temperature, humidity, and wind speed and direction). Regarding the seasonal variation, both VCD and surface concentrations exhibit the same patterns, with a maximum in winter (February) and a minimum in summer (July), in accordance with the large emissions due to domestic heating in winter. The high levels of SO_2 during the cold season are further enhanced by the weakness of the wet deposition mechanism and the frequent temperature-inversion events occurring during this period, favoring the accumulation of SO_2 in the atmospheric layers close to the ground. The variation of the SO_2 amount in Xianghe is also found to be largely driven by wind speed and direction. In the case of east or southwest wind, the VCD at the station rises with the increase of wind speed, since heavy polluting industries are located to the east and southwest and thus the stronger the wind, the more pollution is transported to Xianghe. With respect to the diurnal cycle, larger SO_2 amounts are obtained in the early morning and late evening with a minimum around noon, in line with the diurnal variation of pollutant emission and atmospheric state. Moreover, the diurnal cycle is more pronounced during wintertime, mainly due to the more marked diurnal variation of emission sources and more frequent temperature inversion events during this season.

These three-year MAX-DOAS SO_2 measurements in Xianghe constitute a unique data set for validating and improving space-borne observations over China, which is the region in the world where anthropogenic SO_2 emissions are the largest (Yang et al., 2013; Boynard et al., 2014). In particular, retrieved SO_2 vertical profiles can be used to verify the a priori profile information used in satellite retrievals. Moreover, the combination of both integrated columns and surface concentrations could provide useful information to make explicitly the link between measured satellite columns and surface concentrations.

Acknowledgements. This work was supported by China Scholarship Council, the Special Scientific Research Fund of Meteorological Public Welfare Profession of China (Grant no. GYHY201106045-52), and the National Natural Science Foundation of China (Grant no. 41175030). We also acknowledge the Belgian Federal Science Policy Office, Brussels (AGACC-II project), the EU 7th Framework Programme project NORS (contract 284421), and the ESA CEOS Intercalibration project (ESA/ESRIN Contract 22202/09/I-EC).

References

Bogumil, K., Orphal, J., Homann, T., Voigt, S., Spietz, P., Fleischmann, O. C., Vogel, A., Hartmann, M., Bovensmann, H., Frerik, J., and Burrows, J. P.: Measurements of molecular absorption spectra with the SCIAMACHY Pre- Flight Model: Instrument characterization and reference spectra for atmospheric remote sensing in the 230–2380 nm region, J. Photoch. Photobio. A, 157, 167–184, 2003.

Boynard, A., Clerbaux, C., Clarisse, L., Safieddine, S., Pommier, M., Van Damme, M., Bauduin, S., Oudot, C., Hadji-Lazaro, J., Hurtmans, D., and Coheur, P.-F.: First simultaneous space measurements of atmospheric pollutants in the boundary layer from IASI: a case study in the North China Plain, Geophys. Res. Lett., 41, 645–651, doi:10.1002/2013GL058333, 2014.

Brinksma, E. J., Pinardi, G., Volten, H., Braak, R., Richter, A., Schonhardt, A., van Roozendael, M., Fayt, C., Hermans, C., Dirksen, R. J., Vlemmix, T., Berkhout, A. J. C., Swart, D. P. J., Oetjen, H., Wittrock, F., Wagner, T., Ibrahim, O. W., de Leeuw, G., Moerman, M., Curier, R. L., Celarier, E. A., Cede, A., Knap, W. H., Veefkind, J. P., Eskes, H. J., Allaart, M., Rothe, R.,

Piters, A. J. M., and Levelt, P. F.: The 2005 and 2006 DANDELIONS NO_2 and aerosol intercomparison campaigns, J. Geophys. Res., 113, D16S46, doi:10.1029/2007jd008808, 2008.

Cachorro, V. E., Durán, P., Vergaz, R., and de Frutos, A. M.: Measurements of the atmospheric turbidity of the north-centre continental area in Spain: spectral aerosol optical depth and Ångström turbidity parameters, J. Aerosol Sci., 31, 687–702, 2000.

Chance, K. V. and Spurr, R. J.: Ring effect studies: Rayleigh scattering, including molecular parameters for rotational Raman scattering, and the Fraunhofer spectrum, Appl. Optics, 36, 5224–5230, 1997.

Clémer, K., Van Roozendael, M., Fayt, C., Hendrick, F., Hermans, C., Pinardi, G., Spurr, R., Wang, P., and De Mazière, M.: Multiple wavelength retrieval of tropospheric aerosol optical properties from MAXDOAS measurements in Beijing, Atmos. Meas. Tech., 3, 863–878, doi:10.5194/amt-3-863-2010, 2010.

Eisinger, M. and Burrows, J. P.: Tropospheric sulfur dioxide observed by the ERS-2/GOME instrument, Geophys. Res. Lett., 25, 4177–4180, doi:10.1029/1998GL900128, 1998.

Fioletov, V. E., McLinden, C. A., Krotkov, N., Yang, K., Loyola, D. G., Valks, P., Theys, N., Van Roozendael, M., Nowlan, C. R., Chance, K., Liu, X., Lee, C., and Martin, R. V.: Application of OMI, SCIAMACHY, and GOME-2 satellite SO_2 retrievals for detection of large emission sources, J. Geophys. Res.-Atmos., 118, 11399–11418, doi:10.1002/jgrd.50826, 2013.

Fleischmann, O. C., Hartmann, M., Burrows, J. P., and Orphal, J.: New ultraviolet absorption cross-sections of BrO at atmospheric temperatures measured by time-windowing Fourier transform spectroscopy, J. Photoch. Photobio. A, 168, 117–132, 2004.

Frieß, U., Monks, P. S., Remedios, J. J., Rozanov, A., Sinreich, R., Wagner, T., and Platt, U.: MAX-DOAS O_4 measurements: a new technique to derive information on atmospheric aerosols: 2. Modeling studies, J. Geophys. Res., 111, D14203, doi:10.1029/2005jd006618, 2006.

Frieß, U., Sihler, H., Sander, R., Pöhler, D., Yilmaz, S., and Platt, U.: The vertical distribution of BrO and aerosols in the Arctic: measurements by active and passive differential optical absorption spectroscopy, J. Geophys. Res., 116, D00R04, doi:10.1029/2011JD015938, 2011.

Frins, E., Osorio, M., Casaballe, N., Belsterli, G., Wagner, T., and Platt, U.: DOAS-measurement of the NO_2 formation rate from NO_x emissions into the atmosphere, Atmos. Meas. Tech., 5, 1165–1172, doi:10.5194/amt-5-1165-2012, 2012.

Gauderman, W. J., McConnell, R., Gilliland, F., London, S., Thomas, D., Avol, E., Vora, H., Berhane, K., Rappaport, E. B., and Lurmann, F.: Association between air pollution and lung

function growth in southern California children, Am. J. Resp. Crit. Care., 162, 1383–1390, 2000.
Grainger, J. and Ring, J.: Anomalous Fraunhofer line profiles, Nature, 193, p. 762, 1962.
Großmann, K., Frieß, U., Peters, E., Wittrock, F., Lampel, J., Yilmaz, S., Tschritter, J., Sommariva, R., von Glasow, R., Quack, B., Krüger, K., Pfeilsticker, K., and Platt, U.: Iodine monoxide in the Western Pacific marine boundary layer, Atmos. Chem. Phys., 13, 3363–3378, doi:10.5194/acp-13-3363-2013, 2013.
Heckel, A., Richter, A., Tarsu, T., Wittrock, F., Hak, C., Pundt, I., Junkermann, W., and Burrows, J. P.: MAX-DOAS measurements of formaldehyde in the Po-Valley, Atmos. Chem. Phys., 5, 909–918, doi:10.5194/acp-5-909-2005, 2005.
Hendrick, F., Müller, J.-F., Clémer, K., Wang, P., De Mazière, M., Fayt, C., Gielen, C., Hermans, C., Ma, J. Z., Pinardi, G., Stavrakou, T., Vlemmix, T., and Van Roozendael, M.: Four years of ground-based MAX-DOAS observations of HONO and NO_2 in the Beijing area, Atmos. Chem. Phys., 14, 765–781, doi:10.5194/acp-14-765-2014, 2014.
Hermans, C., Vandaele, A., Fally, S., Carleer, M., Colin, R., Coquart, B., Jenouvrier, A., and Merienne, M.-F.: Absorption cross-section of the collision-induced bands of oxygen from the UV to the NIR, in: Weakly interacting molecular pairs: unconventional absorbers of radiation in the atmosphere, Springer, 193–202, 2003.
Holben, B., Eck, T., Slutsker, I., Tanre, D., Buis, J., Setzer, A., Vermote, E., Reagan, J., Kaufman, Y., and Nakajima, T.: AERONET – a federated instrument network and data archive for aerosol characterization, Remote Sens. Environ., 66, 1–16, 1998.
Hönninger, G., von Friedeburg, C., and Platt, U.: Multi axis differential optical absorption spectroscopy (MAX-DOAS), Atmos. Chem. Phys., 4, 231–254, doi:10.5194/acp-4-231-2004, 2004.
Irie, H., Takashima, H., Kanaya, Y., Boersma, K. F., Gast, L., Wittrock, F., Brunner, D., Zhou, Y., and Van Roozendael, M.: Eight-component retrievals from ground-based MAX-DOAS observations, Atmos. Meas. Tech., 4, 1027–1044, doi:10.5194/amt-4-1027-2011, 2011.
Krotkov, N. A., Carn, S. A., Krueger, A. J., Bhartia, P. K., and Yang, K.: Band residual difference algorithm for retrieval of SO_2 from the aura Ozone Monitoring Instrument (OMI), IEEE T. Geosci. Remote, 44, 1259–1266, 2006.
Lee, C., Martin, R. V., van Donkelaar, A., O'Byrne, G., Krotkov, N., Richter, A., Huey, L. G., and Holloway, J. S.: Retrieval of vertical columns of sulfur dioxide from SCIAMACHY and OMI:

air mass factor algorithm development, validation, and error analysis, J. Geophys. Res., 114, D22303, doi:10.1029/2009JD012123, 2009.
Lee, C., Martin, R. V., van Donkelaar, A., Lee, H., Dickerson, R. R., Hains, J. C., Krotkov, N., Richter, A., Vinnikov, K., and Schwab, J. J.: SO_2 emissions and lifetimes: estimates from inverse modeling using in situ and global, spacebased (SCIAMACHY and OMI) observations, J. Geophys. Res., 116, D06304, doi:10.1029/2010JD014758, 2011.
Li, C., Marufu, L. T., Dickerson, R. R., Li, Z., Wen, T., Wang, Y., Wang, P., Chen, H., and Stehr, J. W.: In situ measurements of trace gases and aerosol optical properties at a rural site in northern China during East Asian Study of Tropospheric Aerosols: an international regional experiment 2005, J. Geophys. Res., 112, D22S04, doi:10.1029/2006JD007592, 2007.
Lin, W., Xu, X., Ge, B., and Liu, X.: Gaseous pollutants in Beijing urban area during the heating period 2007–2008: variability, sources, meteorological, and chemical impacts, Atmos. Chem. Phys., 11, 8157–8170, doi:10.5194/acp-11-8157-2011, 2011.
Ma, J. Z., Beirle, S., Jin, J. L., Shaiganfar, R., Yan, P., and Wagner, T.: Tropospheric NO_2 vertical column densities over Beijing: results of the first three years of ground-based MAX-DOAS measurements (2008–2011) and satellite validation, Atmos. Chem. Phys., 13, 1547–1567, doi:10.5194/acp-13-1547-2013, 2013.
Meller, R. and Moortgat, G. K.: Temperature dependence of the absorption cross sections of formaldehyde between 223 and 323 K in the wavelength range 225–375 nm, J. Geophys. Res., 105, 7089–7101, 2000.
Meng, X., Wang, P., Wang, G., Yu, H., and Zong, X.: Variation and transportation characteristics of SO_2 in winter over Beijing and its surrounding areas, Climatic and Environmental Research, 14, 309–317, 2009 (in Chinese).
Nowlan, C. R., Liu, X., Chance, K. V., Cai, Z., Kurosu, T. P., Lee, C., and Martin, R. V.: Retrievals of sulfur dioxide from the Global Ozone Monitoring Experiment 2 (GOME-2) using an optimal estimation approach: algorithm and initial validation, J. Geophys. Res., 116, D18301, doi:10.1029/2011JD015808, 2011.
Platt, U. and Stuz, J.: Differential Optical Absorption Spectroscopy (DOAS), Principles and Applications, ISBN 978-3-540-21193-8, Springer, Berlin-Heidelberg, 2008.
Rodgers, C. D.: Inverse methods for atmospheric sounding: theory and practice, World Scientific Publishing, Singapore, New Jersey, London, Hong Kong, 2000.
Roscoe, H. K., Van Roozendael, M., Fayt, C., du Piesanie, A., Abuhassan, N., Adams, C., Akrami, M., Cede, A., Chong, J., Clémer, K., Friess, U., Gil Ojeda, M., Goutail, F., Graves, R.,

Griesfeller, A., Grossmann, K., Hemerijckx, G., Hendrick, F., Herman, J., Hermans, C., Irie, H., Johnston, P. V., Kanaya, Y., Kreher, K., Leigh, R., Merlaud, A., Mount, G. H., Navarro, M., Oetjen, H., Pazmino, A., Perez-Camacho, M., Peters, E., Pinardi, G., Puentedura, O., Richter, A., Schönhardt, A., Shaiganfar, R., Spinei, E., Strong, K., Takashima, H., Vlemmix, T., Vrekoussis, M., Wagner, T., Wittrock, F., Yela, M., Yilmaz, S., Boersma, F., Hains, J., Kroon, M., Piters, A., and Kim, Y. J.: Intercomparison of slant column measurements of NO_2 and O_4 by MAX-DOAS and zenith-sky UV and visible spectrometers, Atmos. Meas. Tech., 3, 1629–1646, doi:10.5194/amt-3-1629-2010, 2010.

Tu, F. H., Thornton, D. C., Bandy, A. R., Carmichael, G. R., Tang, Y., Thornhill, K. L., Sachse, G. W., and Blake, D. R.: Long-range transport of sulfur dioxide in the central Pacific, J. Geophys. Res., 109, D15S08, doi:10.1029/2003JD004309, 2004.

Vandaele, A., Simon, P. C., Guilmot, J. M., Carleer, M., and Colin, R.: SO_2 absorption cross section measurement in the UV using a Fourier transform spectrometer, J. Geophys. Res., 99, 25599–25605, 1994.

Vandaele, A. C., Hermans, C., Simon, P. C., Carleer, M., Colin, R., Fally, S., Merienne, M.-F., Jenouvrier, A., and Coquart, B.: Measurements of the NO_2 absorption cross-section from 42 000 cm^{-1} to 10 000 cm^{-1}(238–1000 nm) at 220 K and 294 K, J. Quant. Spectrosc. Ra., 59, 171–184, 1998.

Vlemmix, T., Piters, A. J. M., Stammes, P., Wang, P., and Levelt, P. F.: Retrieval of tropospheric NO_2 using the MAX-DOAS method combined with relative intensity measurements for aerosol correction, Atmos. Meas. Tech., 3, 1287–1305, doi:10.5194/amt-3-1287-2010, 2010.

Wagner, T., Dix, B., von Friedeburg, C., Friess, U., Sanghavi, S., Sinreich, R., and Platt, U.: MAX-DOAS O_4 measurements: a new technique to derive information on atmospheric aerosols – Principles and information content, J. Geophys. Res., 109, D22205, doi:10.1029/2004jd004904, 2004.

Wagner, T., Beirle, S., Brauers, T., Deutschmann, T., Frieß, U., Hak, C., Halla, J. D., Heue, K. P., Junkermann, W., Li, X., Platt, U., and Pundt-Gruber, I.: Inversion of tropospheric profiles of aerosol extinction and HCHO and NO_2 mixing ratios from MAX-DOAS observations in Milano during the summer of 2003 and comparison with independent data sets, Atmos. Meas. Tech., 4, 2685–2715, doi:10.5194/amt-4-2685-2011, 2011.

Wang, T., Nie, W., Gao, J., Xue, L. K., Gao, X. M., Wang, X. F., Qiu, J., Poon, C. N., Meinardi, S., Blake, D., Wang, S. L., Ding, A. J., Chai, F. H., Zhang, Q. Z., and Wang, W. X.: Air quality

during the 2008 Beijing Olympics: secondary pollutants and regional impact, Atmos. Chem. Phys., 10, 7603–7615, doi:10.5194/acp-10-7603-2010, 2010.

Wang, T., Wang, P., Yu, H., Zhang, X., Zhou, B., Si, F., Wang, S., Bai, W., Zhou, H., and Zhao, H.: Intercomparison of slant column measurements of NO_2 by ground-based MAX-DOAS, Acta Phys. Sin., 62, 054206, doi:10.7498/aps.62.054206, 2013.

Wang, T., Wang, P., Yu, H., and Sun, L.: Analysis of the characteristics of tropospheric NO_2 in Xianghe based on MAX-DOAS measurement, Climatic and Environmental Research, 19, 51–60, 2014 (in Chinese).

Wang, W., Chai, F., Zhang, K., Wang, S., Chen, Y., Wang, X., and Yang, Y.: Study on ambient air quality in Beijing for the summer 2008 Olympic Games, Air Qual. Atmos. Healt, 1, 31–36, 2008.

Wittrock, F., Oetjen, H., Richter, A., Fietkau, S., Medeke, T., Rozanov, A., and Burrows, J. P.: MAX-DOAS measurements of atmospheric trace gases in Ny-Ålesund - Radiative transfer studies and their application, Atmos. Chem. Phys., 4, 955–966, doi:10.5194/acp-4-955-2004, 2004.

Wu, F. C., Xie, P. H., Li, A., Chan, K. L., Hartl, A., Wang, Y., Si, F. Q., Zeng, Y., Qin, M., Xu, J., Liu, J. G., Liu, W. Q., and Wenig, M.: Observations of SO_2 and NO_2 by mobile DOAS in the Guangzhou eastern area during the Asian Games 2010, Atmos. Meas. Tech., 6, 2277–2292, doi:10.5194/amt-6-2277-2013, 2013.

Yan, P., Huang, J., and Draxler, R.: The long-term simulation of surface SO_2 and evaluation of contributions from the different emission sources to Beijing city, Sci. China Ser. D, 48, 196–208, 2005.

Yan, P., Wang, X., Wang, Z., and Wu, Q.: Analysis of decreases in NO_2 concentrations during Beijing Olympic Games in 2008, Climatic and Environmental Research, 15, 609–615, 2010 (in Chinese).

Yang, K., Dickerson, R. R., Carn, S. A., Ge, C., and Wang, J.: First observations of SO_2 from satellite Suomi NPP OMPS: widespread air pollution events over China, Geophys. Res. Lett., 40, 4957–4962, doi:10.1002/grl.50952, 2013.

Yu, H., Wang, P., Zong, X., Li, X., and Lü, D.: Change of NO_2 column density over Beijing from satellite measurement during the Beijing 2008 Olympic Games, Chinese Sci. Bull., 55, 308–313, 2010.

Zhao, B., Wang, P., Ma, J. Z., Zhu, S., Pozzer, A., and Li, W.: A high-resolution emission inventory of primary pollutants for the Huabei region, China, Atmos. Chem. Phys., 12, 481–501, doi:10.5194/acp-12-481-2012, 2012.

Table 1. Settings used for the SO_2 and O_4 DOAS analysis.

Parameter	Data source	Fitting intervals (nm)	
		338–370 (O_4)	305–317.5 (SO_2)
NO_2	Vandaele et al. (1998) 220 K, 294 K	x	x (only 294 K)
SO_2	Vandaele et al. (1994) 294 K		x
O_3	Bogumil et al. (2003) 223 K, 243 K	x (only 223 K)	x
O_4	Hermans et al. (2003) 296 K	x	
BrO	Fleischmann et al. (2004) 223 K	x	
H_2CO	Meller and Moortgat (2000) 293 K	x	
Ring	Chance and Spurr (1997)	x	x
Polynomial degree		5	5

Table 2. Error budget of retrieved SO_2 concentration (0–200 m) and VCD.

Uncertainty (%)	Concentration (0–200 m)	VCD
Smoothing + noise errors	13	11
Uncertainty related to aerosols	18	7
Uncertainty related to the a priori	9	17
Uncertainty on SO_2 cross section	5	5
Total uncertainty	24	22

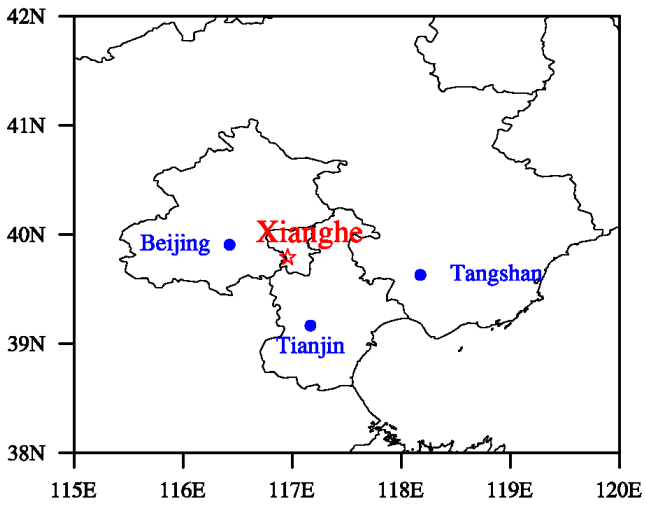

Fig. 1. Location of the Xianghe Observatory and major neighborhood cities.

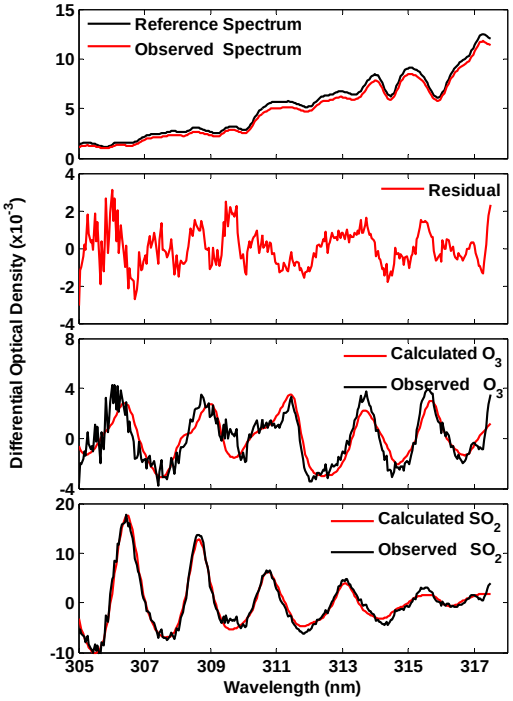

Fig. 2. Example of DOAS fit result for SO_2. It corresponds to 29 September 2010 at 11:20 LT. SZA and EVA values are 43° and 30°, respectively.

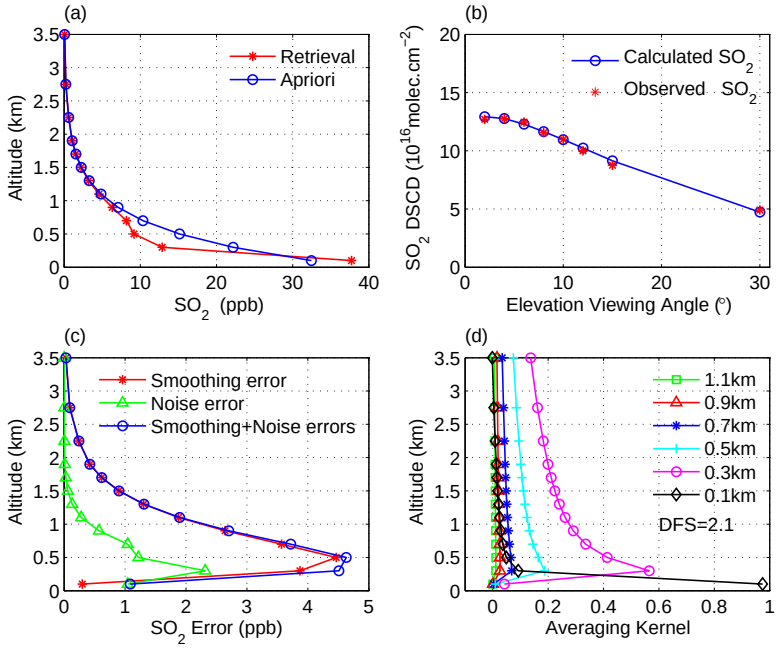

Fig. 3. Example of SO_2 vertical profile retrieval from MAX-DOAS measurements 3 at Xianghe (29 September 2010 at 10:15 LT). **(a)** a priori (blue) and retrieved profile 4 (red); **(b)** observed (red) and calculated (blue) DSCD **(c)** smoothing error (red), noise 5 error (green) and sum of these two (blue); **(d)** averaging kernels.

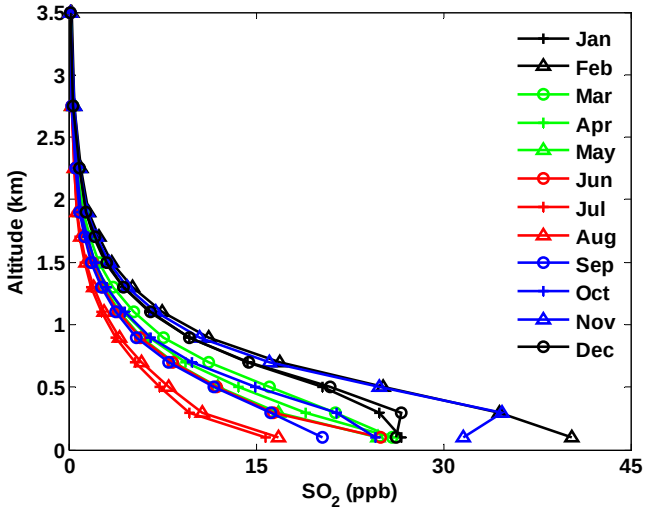

Fig. 4. Monthly-averaged SO_2 concentration vertical profiles for the March 2010–3 February 2013 period.

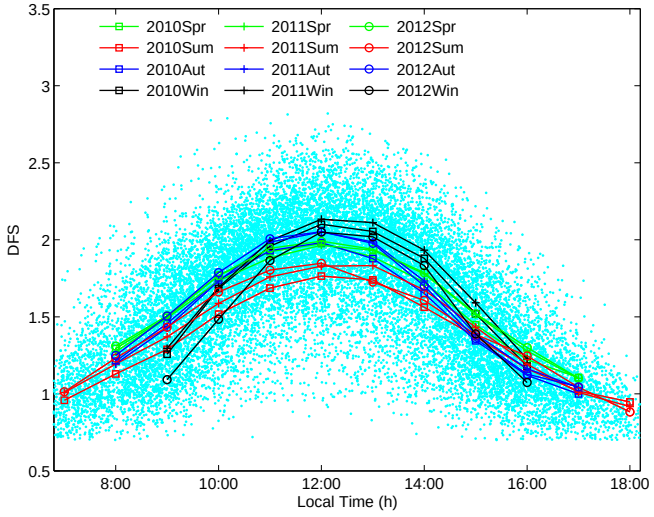

Fig. 5. Seasonally-averaged DFS diurnal cycles corresponding to the SO_2 profile retrievals.

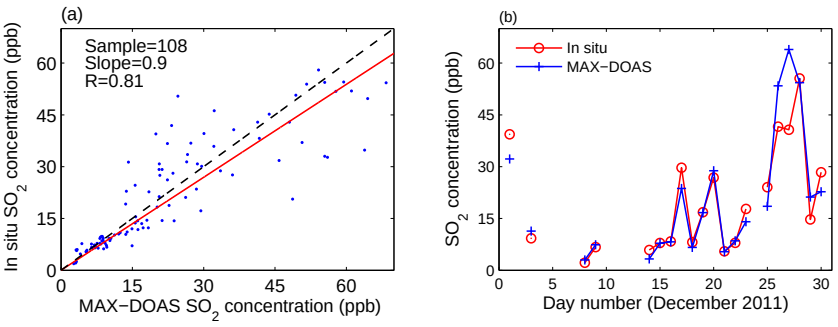

Fig. 6. (a) Scatter plot of in situ SO_2 surface concentrations (0–200 m layer) against MAX-DOAS data for December 2011 (hourly-averaged concentrations). The red line denotes the linear least-squares fit to the data. **(b)** Temporal evolution of daily averaged MAX-DOAS and in situ SO_2 concentrations during December 2011. Gaps in the data series are due to missing MAX-DOAS measurements.

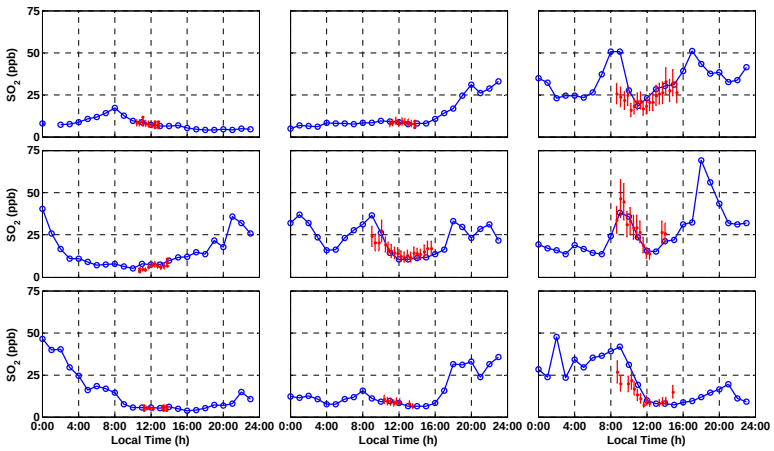

Fig. 7. Comparison between in situ (blue, hourly means) and MAX-DOAS SO_2 surface concentrations (red, each point represents the retrieval from one scan) for the 15–23 December 2011 period (upper plots are for 15–17 December, middle plots is for 18–20 December, lower plots is for 21–23 December).

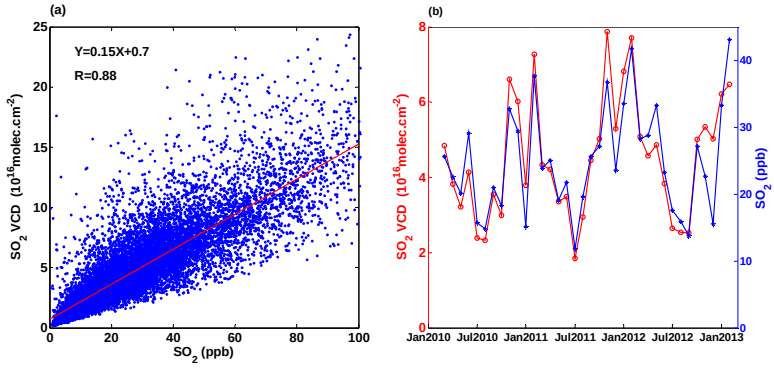

Fig. 8. (a) Scatter plot of SO_2 VCD against surface concentration. The red line represents the linear least-squares fit to the data. **(b)** Temporal evolutions of monthly mean VCD and concentration from March 2010 to February 2013.

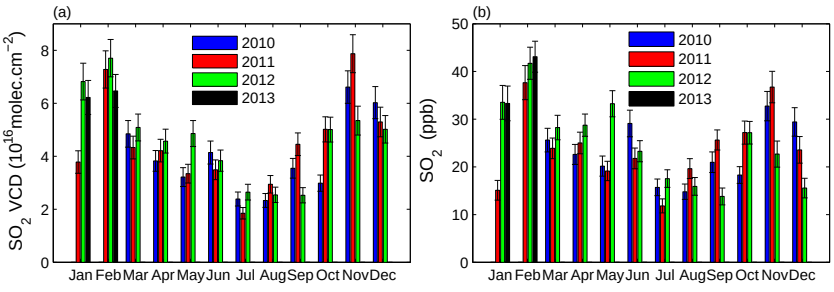

Fig. 9. Monthly mean SO_2 VCD **(a)** and surface concentration **(b)** for the March 2010–February 2013 period.

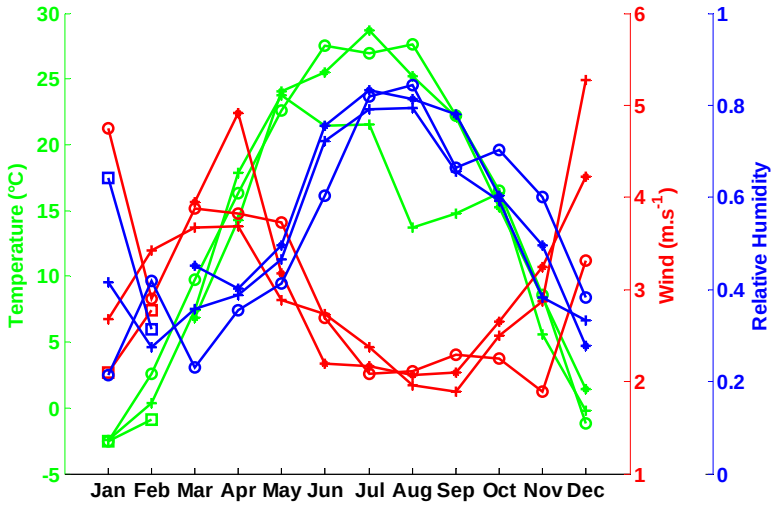

Fig. 10. Seasonal cycles (monthly means) of temperature, humidity, and wind speed in 2010 (marker: star), 2011 (plus), 2012 (circle), and 2013 (square).

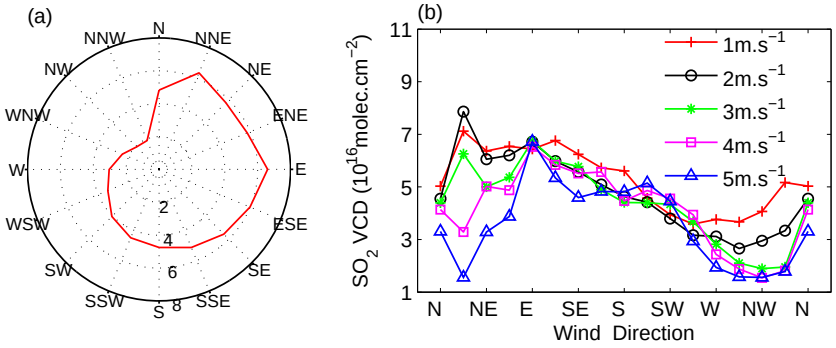

Fig. 11. (a) Wind roses showing the SO_2 VCD (10^{16} molec cm^{-2}) as a function of the wind direction. **(b)** Dependence of SO_2 VCD on wind direction for different wind speeds (from 1 m s^{-1} to 5 m s^{-1} by 1 m s^{-1}).

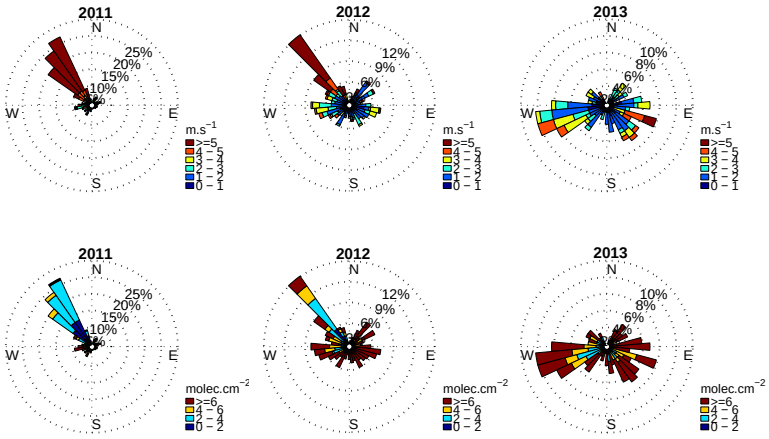

Fig. 12. Wind rose for wind speed (1st row; $m s^{-1}$) and SO_2 VCD (2nd row; 10^{16} molec cm^{-2}) for January 2011 (1st column), 2012 (2nd column), and 2013 (3rd column).

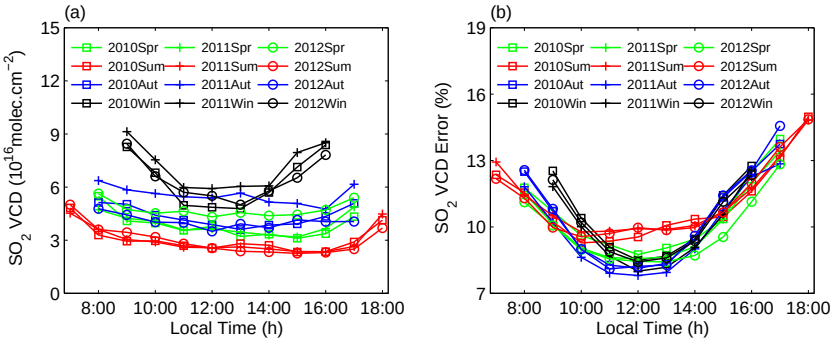

Fig. 13. (a) Seasonally-averaged SO_2 VCD diurnal cycles, and **(b)** corresponding 3 errors. Data points represent hourly means.